Journal of Materials Chemistry C

ROYAL SOCIETY OF CHEMISTRY

PAPER

View Article Online
View Journal | View Issue

Cite this: J. Mater. Chem. C, 2020, 8, 6461

Photochromic fluorescence switching in liquid crystalline polynorbornenes with α-cyanostilbene side-chains†

Yijin Wu, Shasha Zhang, Jiwei Pei and Xiao-Fang Chen *

Received 6th January 2020,
Accepted 25th March 2020

DOI: 10.1039/d0tc00069h

rsc.li/materials-c

Photoresponsive materials have been drawing much attention due to their fast switching properties and non-contact and non-destructive features. In this paper, we report a photoinduced reversible fluorescence switching based on the α-cyanostilbene containing liquid crystalline polynorbornenes. *Z*- and *E*-stereoisomers of α-cyanostilbene monomers with different flexible alkoxy tails and their corresponding *Z*- and *E*-polymers were synthesized and characterized for the first time. P-(*Z*)-345 with three alkoxy tails exhibits a hexagonal columnar structure. P-(*Z*)-4, P-(*Z*)-34, and P-(*Z*)-35 with one or two alkoxy tails possess a lamellar structure. The substitution position and number of alkoxy tails also influence the photoluminescence behaviours, giving rise to different fluorescence colours in bulk. Both monomers and polymers show photoinduced *E*/*Z* isomerization in solution. Under the UV light of 365 nm and 254 nm, polymer thin films or monomer thin films at the noncrystalline state could change their fluorescence colours accordingly, which is mainly due to the photoinduced reversible *E*/*Z* isomerization and [2+2] dimerization in film.

Introduction

Stimulus-responsive materials are generally sensitive to various external signals and release corresponding feedback, exhibiting smart or intelligent behaviours. Among these stimulus sources, materials with photoresponsive character have been drawing much attention due to their fast switching properties and non-contact and non-destructive features.[1–4] Meanwhile, light stimulus sources could be readily controlled and modulated in terms of wavelength, intensity, spatial distribution *etc.*, which produces more delicate and programmable signals to meet advanced applications in future. Until now, most of the photoresponsive materials contain photochromic components, such as diarylethene, spiropyran, and azobenzene. As a consequence of light-triggered *trans–cis* isomerization or ring opening-closure reaction based on photochromic components, photoresponsive materials are able to achieve reversible switching of physical properties, such as colour, geometrical structure, electron conductivity, and dipole interaction.[4] Fluorescence properties could also be modulated either *via* a turn-on/off state or different colour changes in response to light stimuli. The corresponding photoresponsive fluorescent materials have potential applications of photo memory super-resolution imaging, bioimage, logic gate, *etc.*[4–6] Because most of photochromic components are non-fluorescent, photoswitchable fluorescent materials are generally composed of photochromic and luminescent components *via* covalent or non-covalent connection within molecular, polymer or supramolecular systems.[6] Recent studies have revealed that some azobenzene materials show aggregation-induced-emission (AIE) features and can be used as photoswitchable fluorescent materials.[7–9] It still remains a challenge to develop new photoswitching fluorescence systems with controllable and non-destructive response behaviours.

α-Cyanostilbene derivatives[10–13] are known as fluorescent molecules and their AIE properties[14–16] have been studied for the past decade. Recent research revealed that α-cyanostilbene is a good candidate to construct stimulus-responsive materials. The luminescence intensity and colour can be readily modulated under various external stimuli, such as temperature,[17–19] solvent,[20–22] mechanical force,[22–29] and pH.[30] Most of the α-cyanostilbene derivatives are also sensitive to light stimuli. When irradiated by UV light, α-cyanostilbene moiety can undergo *Z*/*E* isomerization[31–44] or [2+2] dimerization,[44–47] which finally influences the conjugation length and the molecular packing.

Key Laboratory of Macromolecular Design and Precision Synthesis, Jiangsu Key Laboratory of Advanced Functional Polymer Design and Application, State and Local Joint Engineering Laboratory for Novel Functional Polymeric Materials, College of Chemistry, Chemical Engineering and Materials Science, Soochow University, Suzhou 215123, P. R. China. E-mail: xfchen75@suda.edu.cn

† Electronic supplementary information (ESI) available: Materials, instruments, and detailed synthetic procedures, ^{1}H NMR spectra of monomers and polymers, DSC thermograms and POM pictures of monomers, AIE properties of monomers and polymers, XRD profiles, UV-vis absorption and fluorescence spectral data. See DOI: 10.1039/d0tc00069h

The fluorescence intensity and colour are thus modulated. Although a variety of responsive properties for α-cyanostilbene derivatives have been explored so far, most of cyanostilbene-related systems are based on small molecules and the reversible switching phenomenon only happens in a limited number of cases. In addition, it should be noted that light-triggered *Z*/*E* isomerization generally takes place in a solution, gel, or liquid crystalline (LC) state, but rarely in a solid crystalline state. α-Cyanostilbene-related materials should be heated to their LC or isotropic phase to realize the light-induced responsive properties in the bulk state. We recently reported a feasible strategy to realize reversible fluorescence switching by incorporating the α-cyanostilbene molecule into a supramolecular polymer system *via* hydrogen bonding interactions.[48] Its fluorescence colour could be changed at room temperature by irradiating 365 nm UV light and reverting to the original state *via* thermal annealing. Recently, an α-cyanostilbene moiety has been reported that could be used as the mesogen to construct fluorescent liquid crystalline polymers,[49–54] but its photo-responsive properties and mechanism in polymer systems have not been revealed until now.

In this work, we successfully realized reversible switching of luminescence colour in α-cyanostilbene-related side-chain LC polymers and the recovery process is readily realized *via* different UV light irradiation at room temperature.

The chemical structures of side-chain polynorbornenes are shown in Scheme 1. The side-chain segment is constructed with the α-cyanostilbene moiety end-attached with various aliphatic tails at different substitution positions. The α-cyanostilbene group has *Z* and *E* configurations. Generally, the *Z*-isomer is the thermally stable one and exhibits a rod-like shape that can act as a calamitic mesogen, while the *E*-isomer adopts a bent-like structure. Photoinduced *E*/*Z* isomerization could simultaneously trigger an LC phase transition and fluorescence switching in some cases. In contrast to the *Z*-isomer, studies of the *E*-isomer are seldom reported, probably due to its lower thermal stability. In this work, we synthesized both *Z*-monomers and *E*-monomers according to the synthetic routes as shown in Scheme 2. The *E*-isomer can be obtained by column chromatography separation from the photo-irradiated *Z*-isomer solution. To keep their configuration in polymer structures, we choose polynorbornene here as the main chain that can be synthesized *via* ring-opening metathesis polymerization (ROMP) under mild conditions.[55] It can be used to avoid thermally induced structural change and to get the corresponding *Z*- and *E*-polymers. Studies of such unique isomer-based polymers would help us to gain more insight

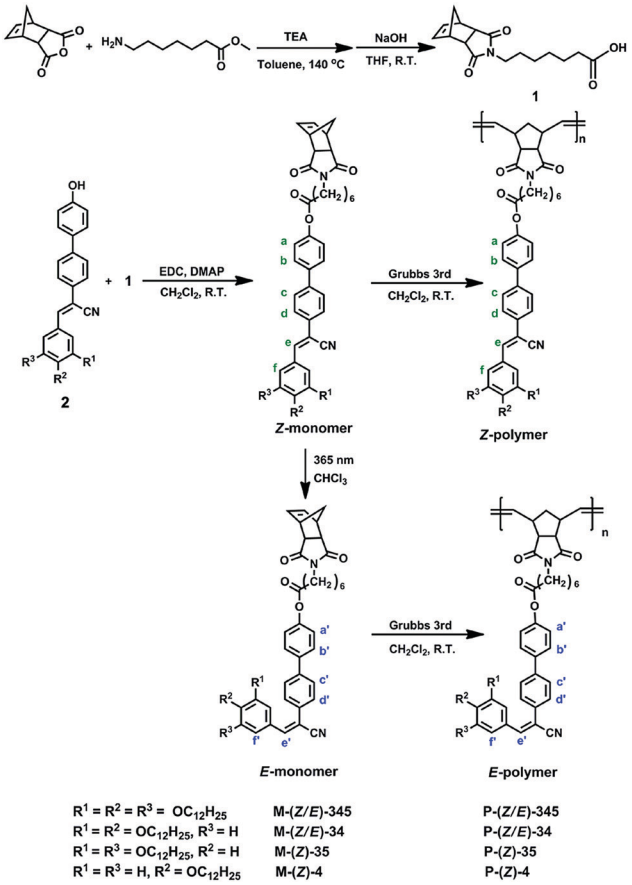

Scheme 2 Synthetic routes for the preparation of the *Z*- and *E*-monomers and their corresponding polymers.

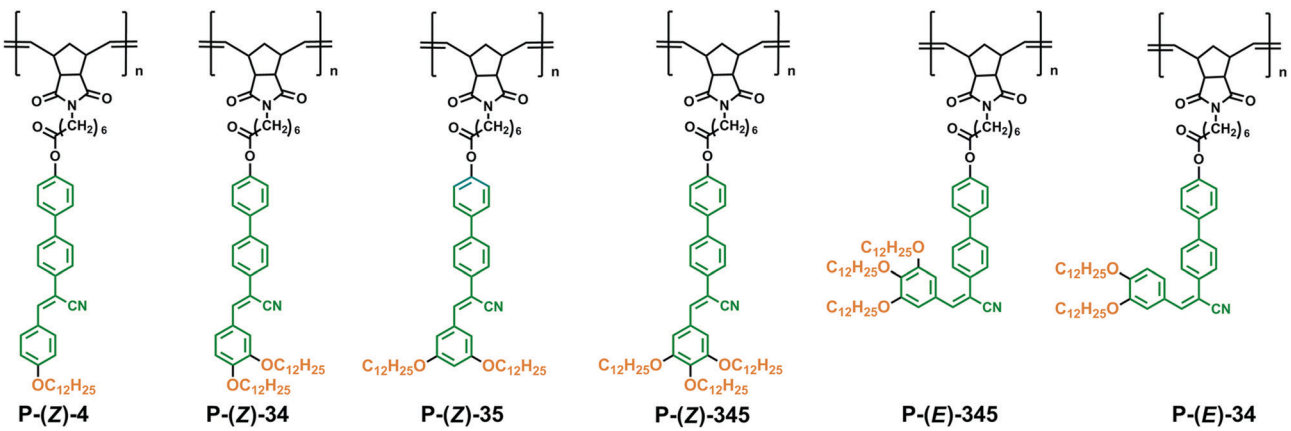

Scheme 1 Chemical structures of polynorbornenes.

into the interplay between the molecular structures (especially the molecular configurations) and self-assembled supramolecular structures. In this system, phase behaviours and the photophysical properties of monomers and polymers either in solution or in the solid state have been systematically studied. The mechanism of photochromic fluorescence switching was also thoroughly investigated.

Results and discussion

Synthesis and characterization of monomers and polymers

Monomers were synthesized according to the synthetic route as shown in Scheme 2. The detailed synthetic procedures are provided in the ESI.† By irradiating a *Z*-monomer solution ($CHCl_3$, 1×10^{-5} mol L^{-1}) with 365 nm UV light from a hand-held UV light (1.0 mW cm^{-2}), its UV-vis absorption spectrum changed instantly. The absorption maximum of M-(*Z*)-345 (Fig. 1a) showed a hypsochromic shift from 361 nm to 348 nm after 150 s UV irradiation and the absorbance decreases as a function of the exposure time. Similar changes could also be found in other monomers. Further investigation was carried out by ^{1}H NMR spectroscopy to monitor the structural change during UV irradiation. ^{1}H NMR spectra (Fig. 1b) clearly show that an UV-induced *Z* to *E* isomerization was taking place. The content of M-(*E*)-345 gradually increased in $CDCl_3$ solution, together with the decrease of M-(*Z*)-345 content. After 2 h irradiation, the $CDCl_3$ solution of M-(*Z*)-345 (10 mg mL^{-1}) in the NMR tube reached a photostationary state. The maximum photoconversion from *Z* to *E* was calculated from the ^{1}H NMR spectra, which is as high as 82%. Apart from *Z* to *E* isomerization, no other photoreaction was detected in $CDCl_3$ solution.

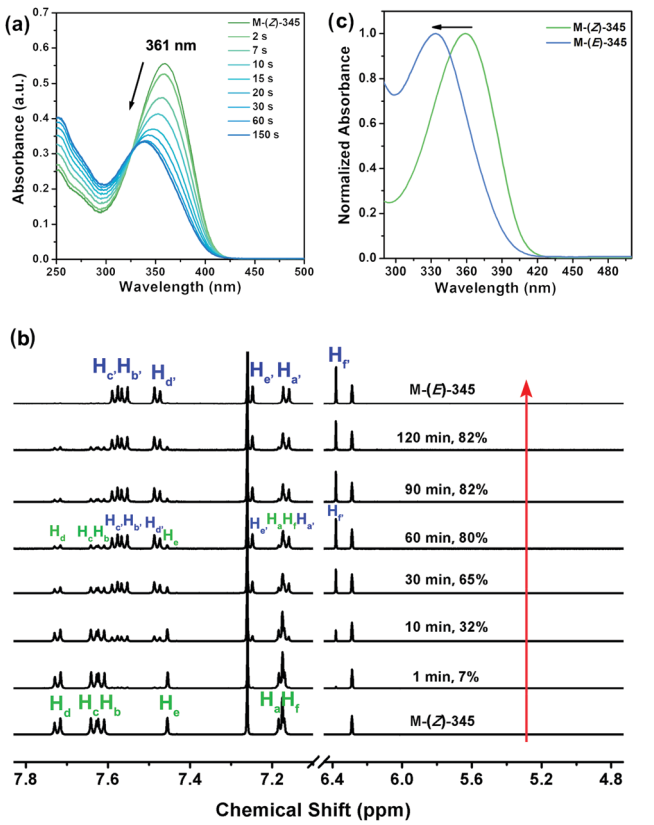

Fig. 1 (a) UV-vis absorption spectra of M-(*Z*)-345 in $CHCl_3$ (1×10^{-5} mol L^{-1}) before and after irradiation upon 365 nm UV light with increasing illumination times; (b) ^{1}H NMR spectra of M-(*Z*)-345 before and after 365 nm UV irradiation with different illumination times and pure M-(*E*)-345; (c) UV-vis absorption spectra of pure M-(*Z*)-345 and M-(*E*)-345 in $CHCl_3$ solution.

The *E*-monomer could be successfully separated and purified from the corresponding irradiated *Z*-monomer solution *via* column chromatography (Scheme 2). Chemical structures of both *Z*- and *E*-monomers were verified *via* ^{1}H NMR (Fig. 1b and Fig. S1–S4, ESI†), ^{13}C NMR, high-resolution MS and elemental analysis. Compared to the UV spectrum of M-(*Z*)-345, the λ_{max} of M-(*E*)-345 is blue shifted to 334 nm as shown in Fig. 1c, due to its bent structure with relatively short conjugation.

The ROMP was carried out at room temperature in CH_2Cl_2 solution for 4 h. Both *Z*-monomers and *E*-monomers can be polymerized under this condition with high conversion. During polymerization, the Schlenk tube was wrapped with aluminium foil to avoid light-induced isomerization. ^{1}H NMR spectra in Fig. 2 confirm that both P-(*Z*)-345 and P-(*E*)-345 are synthesized successfully with their side chains keeping the same configurations as the corresponding monomers and no other reactions take place during polymerization. The ^{1}H NMR spectra of other polymers can be found in Fig. S2–S4 (ESI†). Their molecular weights and polydispersity values were measured *via* GPC with polystyrene standards. The M_n values of polymers, as shown in Table 1, are higher than 4×10^4 g mol^{-1} with relatively narrow polydispersity.

Phase behaviours of monomers and polymers

The mesomorphic properties of monomers and polymers were investigated with the combination of polarized optical microscopy (POM), differential scanning calorimetry (DSC), small-angle X-ray scattering (SAXS) and wide-angle X-ray scattering (WAXS). All *Z*-monomers, which contain rigid rod-like structures, show enantiotropic LC behaviours, whereas *E*-monomers exhibit only crystalline behaviours. Their DSC curves and POM pictures could be found in the ESI† (Fig. S5–S6). The TGA results of

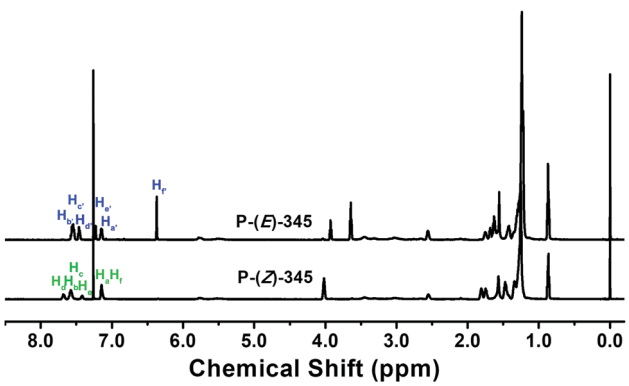

Fig. 2 ^{1}H NMR spectra of P-(*Z*)-345 and P-(*E*)-345.

Table 1 Molecular weight and thermal behaviours characterization of the polymers

Polymer	M_n[a] (g mol^{-1})	M_w[a] (g mol^{-1})	PDI[a]	T_d[b] (°C)	T_i[c] (°C)
P-(*Z*)-345	102 600	126 600	1.23	372	182
P-(*E*)-345	86 400	124 400	1.44	361	—
P-(*Z*)-34	85 300	110 300	1.29	390	227
P-(*E*)-34	48 400	84 700	1.75	385	—
P-(*Z*)-35	103 500	123 600	1.19	396	148
P-(*Z*)-4	86 600	109 300	1.26	379	230

[a] Determined by GPC in THF using polystyrene standards. [b] 5% weight loss temperature evaluated by TGA under a nitrogen atmosphere at a heating rate of 10 °C min^{-1}. [c] Isotropization temperature confirmed by DSC at a heating rate of 10 °C min^{-1}.

polymers listed in Table 1 show the decomposition temperature is over 310 °C when the sample reaches 5% weight loss under a nitrogen atmosphere. Therefore, further phase behaviour studies of these polymers were conducted below this temperature. Fig. 3a displays DSC curves of *Z*-polymers recorded during the second heating and the subsequent cooling process. A small endothermic peak in the heating curve and a corresponding exothermic peak in the cooling process for each *Z*-polymer can be found, indicating the existence of phase transition. The phase transition process is also studied *via* POM. At first, *Z*-polymers exhibit birefringence. When the sample is heated above the phase transition temperature, it enters an isotropic state. Then after cooling the sample, the birefringence appears again. As shown in Fig. 3b characteristic LC textures could gradually grow up when the sample is cooled slowly from the isotropic state. P-(*Z*)-345 shows a typical fan-like texture. P-(*Z*)-4, P-(*Z*)-34 and P-(*Z*)-35 just show a granular texture due to their high viscosity. Therefore, the isotropic temperature T_i was consistent with the phase transition temperature detected *via* DSC, which is listed in Table 1. Combined with DSC and POM results, the T_i is associated with the number of substituted aliphatic chains. The mono-substituted P-(*Z*)-4 has the highest T_i at 230 °C. P-(*Z*)-35 has the lowest T_i, which is due to the plasticization of flexible aliphatic tails and the meta-substituted position, which decrease the intermolecular interaction of rigid mesogens to some extent.

A SAXS method was further performed to verify the LC structure of these polymers. As shown in Fig. 3c, the SAXS profile of P-(*Z*)-4 shows three diffraction peaks in the low-angle region with the *q* ratio of 1 : 2 : 3, which refers to a long-range ordered lamellar structure. The calculated layer thickness (*L*) is 7.31 nm. Meanwhile, only a broad scattering peak exists in the wide-angle region in Fig. 3d, indicating no positional order within the layer. When the rigid mesogen is attached with two aliphatic tails at the 3,4 or 3,5 positions, the corresponding P-(*Z*)-34 and P-(*Z*)-35 keep lamellar structures with the layer thickness around 6.22 and 6.04 nm, respectively. The layer thickness is associated with the length of the repeating unit in side-chain liquid crystal polymers (SCLCPs), based on the general schematic packing model presented in Fig. 3e. The calculated length (L_c) of an extended repeating unit structure with an all-*trans* conformation of the aliphatic chain is around 4.45 nm. Since *L* should not be larger than $2L_c$ in the lamellar

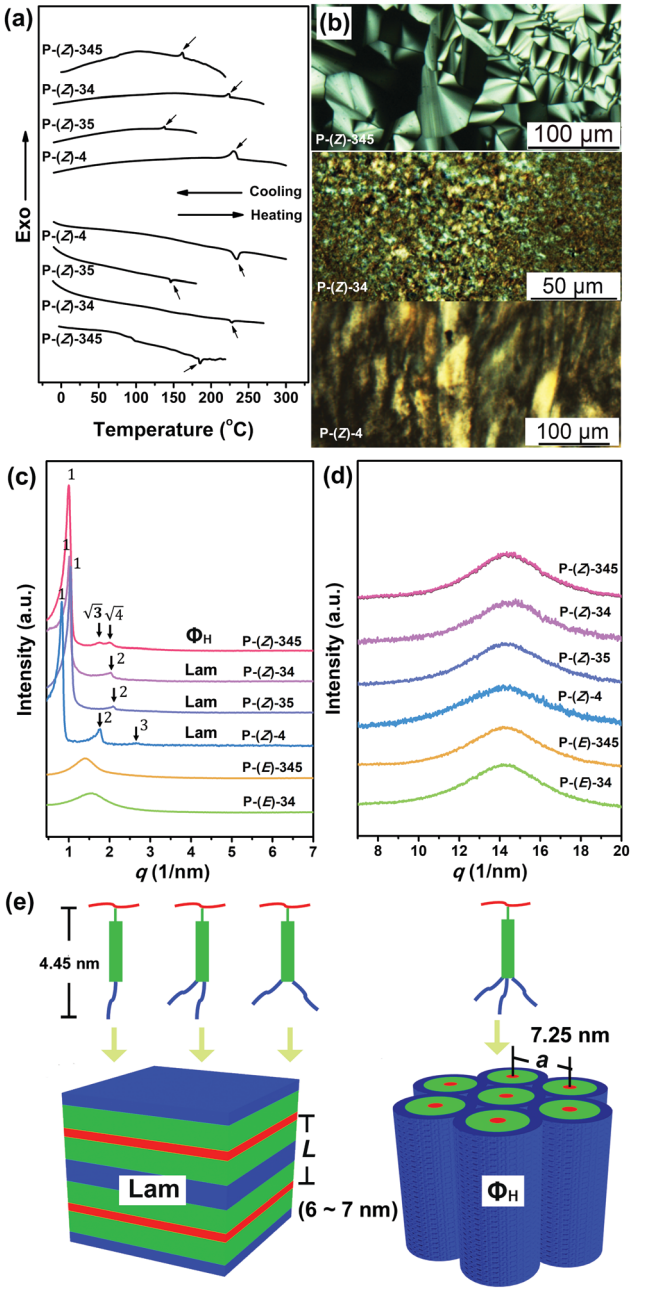

Fig. 3 (a) DSC curves of polymers at a heating and cooling rate of 10 °C min^{-1}. (b) POM pictures of P-(*Z*)-345 at 150 °C, P-(*Z*)-34 at 201 °C and P-(*Z*)-4 at 210 °C. SAXS (c) and WAXS (d) profiles of thermally annealed polymers recorded at room temperature. (e) schematic illustration of the phase structure model of smectic and Φ_H phases.

structure, the side chain adopts a partially interdigitated packing model within each layer in this case. When the cyano-stilbene mesogen was attached with three aliphatic chains at the 3, 4, and 5 positions, the corresponding polymer P-(*Z*)-345 exhibited the other type of ordered structure. The SAXS profile of the thermally annealed sample showed three diffraction peaks with the *q* in a ratio of $1:\sqrt{3}:2$. A typical hexagonal columnar (Φ_h) structure with the lattice parameter of a = 7.25 nm was confirmed. The POM picture in Fig. 3b presents

the characteristic fan-like texture of a columnar phase for P-(*Z*)-345, which is also consistent with the SAXS result. The substituent position and number of aliphatic tails affect the LC structure to some extent.

Phase structures of the corresponding *E*-polymers have also been studied. The cyanostilbene segment here adopts a bent structure instead of a rod-shaped one. In contrast to *Z*-polymers, SAXS profiles of both P-(*E*)-4 and P-(*E*)-345 only show a broad peak in the low angle region (Fig. 3c). Meanwhile, no phase transition and birefringence could be detected for *E*-polymers, indicating the amorphous nature. It is well known that the rod-like shape of the mesogens is important for the stabilization of the lamellar structure in SCLCPs. In this system, neither a lamellar nor columnar structure could be maintained when the cyanostilbene segment changes from a *Z* to *E* configuration. The conformation of the cyanostilbene segment in this system plays a virtual role in the formation of the LC phase. Meanwhile, the aliphatic chain could be used to modulate the phase transition temperatures and phase structures. Based on the result, it could be speculated that if photoinduced *Z* to *E* isomerization could be triggered in the bulk state, an LC-to-iso phase transition would be taking place in this system.

Photophysical properties of monomers and polymers

The UV-vis absorption spectra of monomers in dilute $CHCl_3$ solution (1×10^{-5} mol L^{-1}) are shown in Fig. 4a. The maximum absorption peaks of M-(*Z*)-345, M-(*Z*)-34, M-(*Z*)-35, and M-(*Z*)-4 are at 359 nm, 360 nm, 339 nm, and 351 nm, respectively. As we have mentioned, M-(*E*)-345, the corresponding *E*-isomer, could be found with a notable blue shift of 25 nm (Fig. 1c), as is M-(*E*)-34, which is at 343 nm as shown in Fig. S7a (ESI†). Meanwhile, the UV-vis absorption spectra of the corresponding polymers are similar to the corresponding monomers (Fig. S8, ESI†). The photoluminescence (PL) spectra of monomers in $CHCl_3$ solution (1×10^{-5} mol L^{-1}) are shown in Fig. 4b. The emission peak of each monomer is quite close to each other, which is located around 447 nm. Cyanostilbene derivatives are known as AIEgens. *Z*-Monomers, which contain cyanostilbene segments, also retain the characteristic AIE properties. The PL intensity shows a dramatic change from THF solution to the strongly fluorescent aggregates in THF/water mixtures. As shown in Fig. 4c, M-(*Z*)-345 is almost nonluminescent in pure THF and the fluorescence intensity remains almost unchanged in the THF/water mixtures with up to 50% (f_w). However, there is a sharp increase when the water content reaches 60%. With up to 60% water content, these molecules begin to form aggregates, and the emission band shows an obvious red-shift from 447 nm to 483 nm. Other *Z*-monomers also exhibit a dramatic increase of PL intensity in THF/water mixtures (Fig. S7, ESI†).

In the solid state, the molecular packing influences the PL spectra. As shown in Fig. 4d, the maximum emission wavelengths of *Z*-monomers are 481 nm (M-(*Z*)-345), 484 nm (M-(*Z*)-34), 459 nm (M-(*Z*)-35), and 463 nm (M-(*Z*)-4). All *Z*-monomers contain the identical cyanostilbene segment, but with a substituted dodecanoxyl chain at different positions. Comparing the PL spectra of M-(*Z*)-345 in solution (Fig. 4b) and in the solid state (Fig. 4d), it is clearly seen that the aliphatic chains have less effect on the fluorescence properties in solution, but really affect the PL properties in the condensed state,[56] especially for M-(*Z*)-345 and M-(*Z*)-34, both of which exhibit an obvious red-shift. The quantum yield (Φ_f) of monomers in solution is very low, exhibiting non-fluorescence, while they show high fluorescence properties in the solid state with high Φ_f (>50%).

Polymers also retain AIE properties. Taking P-(*Z*)-345 as an example, the PL intensity gradually increases upon the continuous addition of water in THF/water mixed solvents accompanied by a red-shift of maximum emission wavelength as shown in Fig. 5a, indicating the gradual formation of aggregates. As mentioned above, in the case of M-(*Z*)-345, when f_w exceeded 60%, the fluorescence intensity was dramatically increased. But for polymers, the aggregates form more easily when f_w reaches only 10%. Fig. 5b presents the PL change as a function of water content for both M-(*Z*)-345 and P-(*Z*)-345. The increase of PL intensity and the red-shift of wavelength of P-(*Z*)-345 are gentler than that of the monomer M-(*Z*)-345. Although M-(*Z*)-345 and P-(*Z*)-345 have the same concentration of cyanostilbene segment in THF, the concentration of cyanostilbene around the polymer chain is much higher than that in other places in dilute solution, which provides much higher propensity to aggregate with less water content. Other polymers exhibit similar AIE behaviours in THF/water mixtures (Fig. S8, ESI†).

These polymers can still undergo *Z*/*E* isomerization in $CHCl_3$ solution under the irradiation of 365 nm UV light, which was confirmed *via* UV-vis absorption and ^{1}H NMR spectra (Fig. S9, ESI†). The time to reach the equilibrium of *Z*/*E* isomerization for P-(*Z*)-345 is longer than that of M-(*Z*)-345. It is also due to

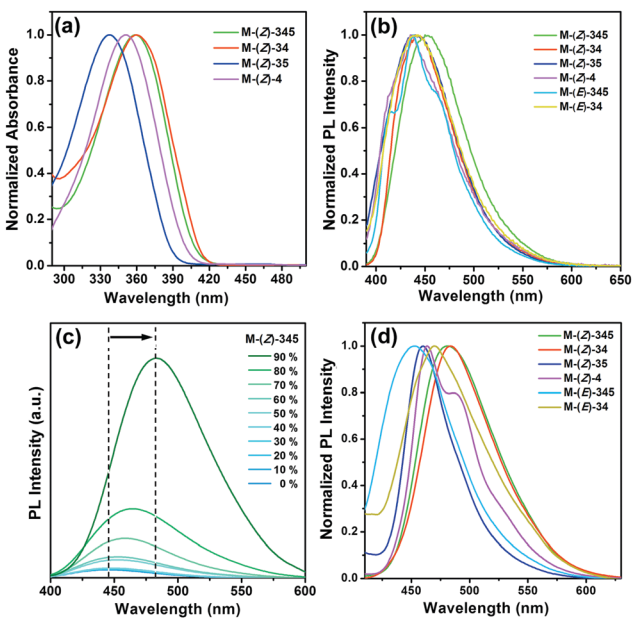

Fig. 4 (a) UV-vis absorption spectra of monomers in $CHCl_3$ (1×10^{-5} mol L^{-1}). (b) PL spectra of monomers in $CHCl_3$ (1×10^{-5} mol L^{-1}). (c) PL spectra changes of M-(*Z*)-345 depending on the water fractions in THF. (d) Fluorescence spectra of monomers in the solid state.

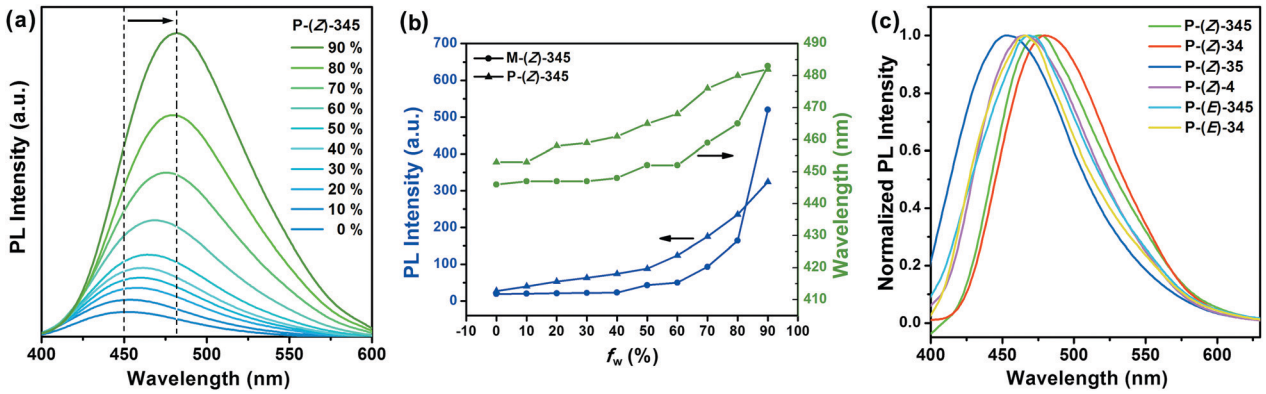

Fig. 5 (a) PL spectral changes of P-(*Z*)-345 depending on the water fractions in THF. (b) PL intensity and wavelength of M-(*Z*)-345 and P-(*Z*)-345 as a function of water content (f_w) in THF/water mixtures. (c) PL spectra of polymer films.

the same reason that the presence of the polymer backbone causes the higher local concentration of the cyanostilbene segment than that of the corresponding monomer solution.

PL spectra of polymers at the solid state are shown in Fig. 5c. The emission peaks of polymers are similar to those of the corresponding monomers, which means that PL properties could be kept after polymerization in these systems. After polymerization, the Φ_f of polymer samples is decreased due to the noncrystalline feature of polymers.

Photochromic fluorescence switching in monomer and polymer films

The fluorescence modulation properties of polymers and monomers have been investigated. For example, the P-(*Z*)-345 film was prepared on a quartz plate *via* a spin-coating method. As shown in Fig. 6a, the original film emitted green fluorescence with the maximum emission wavelength of 476 nm. Upon 365 nm UV irradiation, the wavelength of emission blue shifted gradually. After 30 min, the PL peak position shifts to 462 nm and then remains constant with further UV irradiation. The recovery process has been realized *via* thermal annealing. In this work, the irradiated P-(*Z*)-345 film here is quite hard to convert to its original state using a heating process alone. The intriguing thing is that the luminescence colour of the irradiated film can be restored to its original state by shedding the light of 254 nm at room temperature. As shown in Fig. 6b, after 10 min the emission peak red shifts to 472 nm. This means that the reversible fluorescence switching could be realized in the polymer film only by using UV light stimuli with a different wavelength. Because the luminescence colour is quite different before and after UV irradiation, the fluorescence patterns with dual emission colours could be easily obtained by carrying out 365 nm UV irradiation for 30 min through a mask. Fig. 6c presents the writing-erasing cycles of fluorescence images in a P-(*Z*)-345 film. The fluorescence pattern could be erased upon 254 nm UV irradiation, and then the whole film shows a green colour again. Different patterns could be written again in the same film by using different masks as shown in Fig. 6c.

A similar responsive process was also found in the as-prepared monomer thin film, but it should be noted that the monomer film easily appeared to be heterogeneous after several irradiation cycles. The freshly prepared M-(*Z*)-345 film

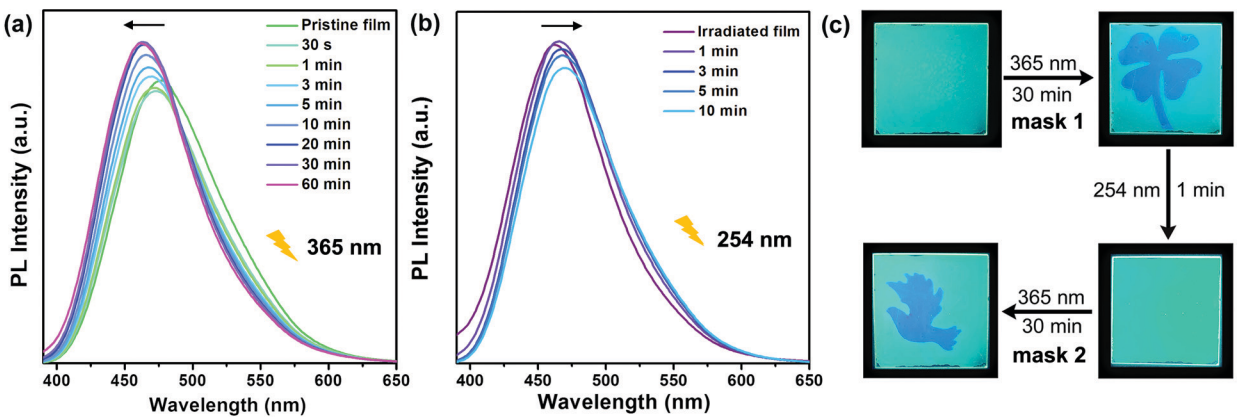

Fig. 6 (a) PL spectra of the P-(*Z*)-354 film irradiated with 365 nm UV light for different exposure times. (b) PL spectra of the irradiated P-(*Z*)-354 film further irradiated with 254 nm UV light for different exposure times. (c) Fluorescent pictures of the P-(*Z*)-345 film irradiated with 365 nm UV light and then with 254 nm light.

showed a noncrystalline state and slowly entered a crystalline state as revealed *via* XRD experiments (Fig. S10, ESI†). After crystallization, the monomer film did not show any photo-responsive behaviours, which was confirmed *via* ^{1}H NMR measurements. There were no significant differences found between the results in the ^{1}H NMR spectra before and after irradiation (Fig. S11, ESI†).

In order to study the mechanism of fluorescence switching, ^{1}H NMR was first carried out to detect the chemical structural change of the polymer before and after UV irradiation. However, the film of P-(*Z*)-345 became difficult to dissolve in most organic solvents after UV illumination. It was speculated that some cross-linking reactions might occur in the film. As mentioned above, the as-prepared non-crystallized monomer film has similar photostimulus-responsive properties. Thus, the corresponding monomer was chosen instead to track the photoinduced switching behaviours. After 365 nm UV irradiation for 30 min, the M-(*Z*)-345 film was dissolved in $CDCl_3$ for the ^{1}H NMR measurements. First of all, signals belonging to the *E*-isomer could be clearly detected *via* ^{1}H NMR as shown in Fig. 7. This means that the *E*/*Z* isomerization could take place in the bulk state. Besides the *E*-isomer, the ^{1}H NMR spectra of the irradiated samples also show two new singlets at 4.95 and 5.09 ppm (Fig. 7). As reported before,[45–47] when cyano-substituted cyclobutanes are generated *via* photocycloaddition, one singlet in the ^{1}H NMR at around 5 ppm could be detected. In this case, the ^{1}H NMR result indicates that at least two types of cyclobutanes appeared in the thin film after UV irradiation. Here we assign the singlet at 4.95 nm to dimer 1 and the other singlet to dimer 2 (Fig. 7). The content ratio of the integrated peaks of the two singlets in irradiated film is related to the temperature. When the film was irradiated at room temperature, both dimers 1 and 2 could be detected. The content of dimer 1 decreased with increasing temperature. When it was irradiated at 75 °C, only dimer 2 existed, which was confirmed *via* ^{1}H NMR (Fig. 7). Then dimer 2 was successfully separated from the mixture through column chromatography (Fig. 8a).

We also got the irradiated sample that mainly contained dimer 1 rather than dimer 2 *via* controlling the temperature

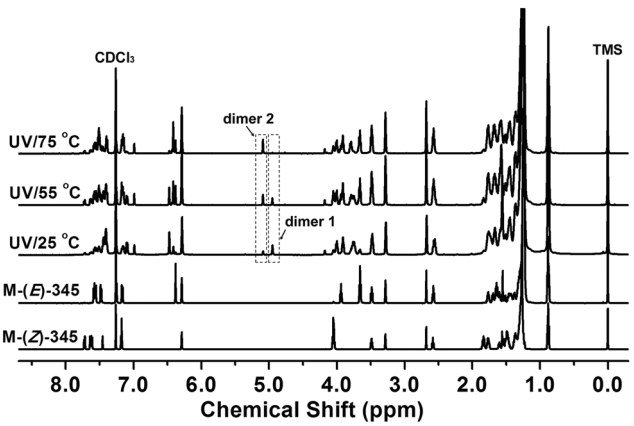

Fig. 7 ^{1}H NMR spectra of M-(*Z*)-345, M-(*E*)-345 and the as-casted film of M-(*Z*)-345 irradiated with 365 nm UV light at 25, 55 and 75 °C for 30 min.

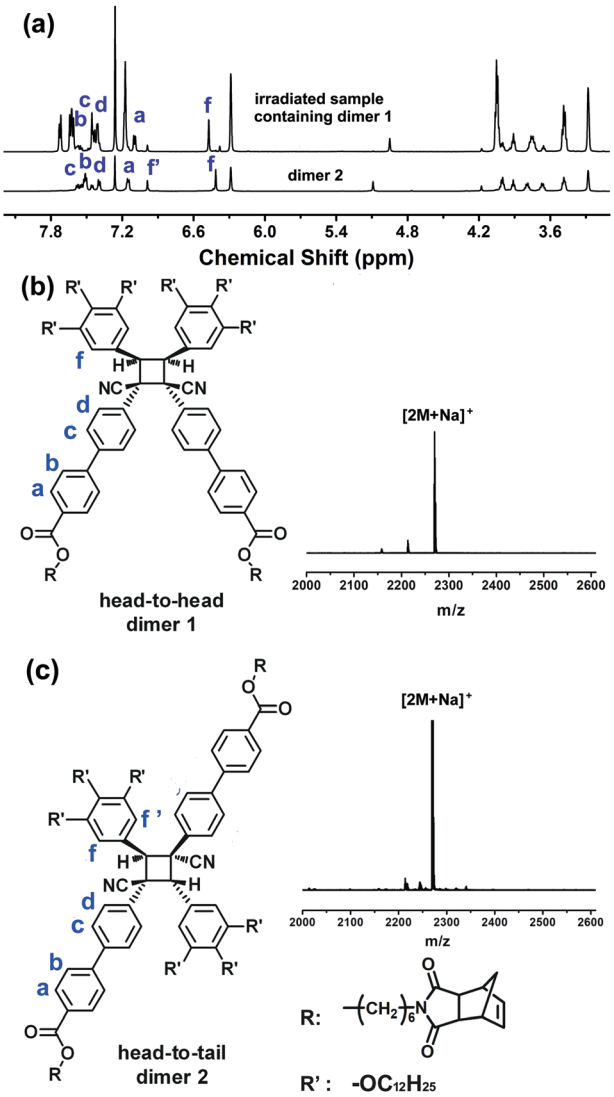

Fig. 8 (a) ^{1}H NMR spectra of the irradiated sample containing dimer 1 and purified dimer 2.; Chemical structures and corresponding MS spectra of dimer 1 (b) and dimer 2 (c).

and the irradiation time (Fig. 8a). The chemical structures and the stereochemistry of the major cyclobutanes formed in this photoprocess of these two dimers were studied *via* 2D ^{1}H NMR experiments. Based on rotational frame nuclear Overhauser effect spectroscopy (ROESY) and H–H correlation spectroscopy (COSY) experiments (Fig. S12, ESI†), dimer 2 adopts a head-to-tail structure and dimer 1 possesses a head-to-head structure. Their MS spectra shown in Fig. 8b and c also confirm the formation of the dimers. Based on this result, we could also speculate that the molecules tend to adopt head-to-head packing in the non-crystalline phase, which can be a bilayer lamellar structure or a columnar structure. When heating close to the isotropic state, molecules generally adopt a more interdigitated arrangement and head-to-tail dimers become dominant.

The content ratio of the *Z*-isomer, *E*-isomer, dimer 1 and 2 in the irradiated film could also be measured *via* ^{1}H NMR. As shown in Fig. 9, after irradiation *via* 365 nm UV light, the

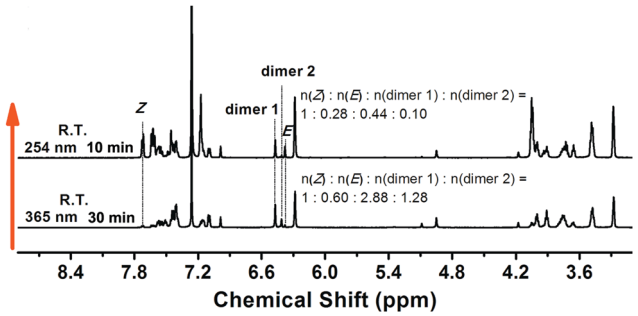

Fig. 9 ^{1}H NMR of M-(*Z*)-345 film after irradiating with 365 nm UV light for 30 min and then irradiating with 254 nm UV light for 10 min.

molar content ratio of the *n*(*Z*-isomer) : *n*(*E*-isomer) : *n*(dimer 1) : *n*(dimer 2) in the film is 1 : 0.60 : 2.88 : 1.28, which means that both *E*/*Z* isomerization and [2+2] cycloaddition take place within the film and most of the *Z*-isomer turns to *E*-isomer and dimers by irradiation *via* 365 nm. As a consequence of the UV-induced structural change, a blue shift of the PL peak from 476 nm to 462 nm was detected (Fig. 6a). Then, by subsequent irradiation *via* 254 nm UV light, the fluorescence colour of the film reverted to the green one. In this state, the content molar ratio of the major components *n*(*Z*-isomer) : *n*(*E*-isomer) : *n*(dimer 1) : *n*(dimer 2) was measured as 1 : 0.28 : 0.44 : 0.10. The content of *Z*-isomer increased again.

The confirmation of dimers in the irradiated monomer film can also answer the question of whether the polymer thin film becomes insoluble in organic solvents after 365 nm UV irradiation. The cycloaddition may take place as well within the cyanostilbene side chains to cross-link the polymer thin film. Then, the 254 nm UV light can act as a decrosslinking effect and make the blue fluorescent film return to its original green luminescence colour, accompanied with improved solubility. Other *Z*-polymers exhibit similar photochromic fluorescence switching behaviours at room temperature (Fig. S13, ESI†).

As we discussed above, *Z*-polymers are liquid crystalline polymers, while *E*-polymers are amorphous; the possibility of a photoinduced phase transition from the LC phase to the isotropic phase is also studied. In this work, both *E*/*Z* isomerization and [2+2] dimerization are detected in the LC phase, based on the results of Fig. 9. The photoreaction is more complicated than that of azobenzene materials.[57,58] We studied the phase transition of the irradiated polymer film *via* POM. The irradiated zone has a relatively lower isotropization temperature than the unirradiated zone, but because the irradiated zone is partially crosslinked due to [2+2] dimerization, a weak birefringence could still be observed.

Conclusions

In summary, we designed and synthesized a set of side-chain liquid crystalline polynorbornenes. Each side chain contains an α-cyanostilbenic moiety with end-attached aliphatic tails with controlled substituent number and position. Both *Z*- and *E*-monomers could be prepared and could be polymerized *via* ROMP at room temperature. *Z*-Polymers exhibit LC behaviours. P-(*Z*)-4, P-(*Z*)-34, and P-(*Z*)-35 possess lamellar structures. P-(*Z*)-345 possesses a Φ_h structure. The corresponding *E*-polymers show amorphous behaviours. All *Z*-polymers show AIE and photo-responsive properties. Both *Z*-monomers and polymers show *Z* to *E* isomerization in solution when irradiated *via* 365 nm UV light. In non-crystalline thin films, photochromic fluorescence switching is triggered *via* different UV lights. The products both from *E*/*Z* isomerization and [2+2] cyclodimerizaiton are detected. This responsive behaviour is reversible by changing only the wavelength of irradiated light. It provides a unique opportunity to realize fluorescence colour switching under mild conditions.

In conclusion, this work presents a useful strategy toward the combination of photochromic fluorescence switching and liquid crystalline polymers through molecular design. Further investigation on controllable colour switching and modulation in liquid crystalline systems *via* all-light stimuli is still ongoing.

Conflicts of interest

There are no conflicts to declare.

Acknowledgements

This work was supported by the National Natural Science Foundation of China (No. 21474073, 21875157, and 21174003) and the Priority Academic Program Development of Jiangsu Higher Education Institutions (PAPD). We thank Beamline BL16B1 at SSRF for providing the beamtime.

References

1 J. Zhang, Q. Zou and H. Tian, *Adv. Mater.*, 2013, **25**, 378–399.
2 H. N. Kim, Z. Guo, W. Zhu, J. Yoon and H. Tian, *Chem. Soc. Rev.*, 2011, **40**, 79–93.
3 H. K. Bisoyi and Q. Li, *Chem. Rev.*, 2016, **116**, 15089–15166.
4 F. Ercole, T. P. Davis and R. A. Evans, *Polym. Chem.*, 2010, **1**, 37–54.
5 I. Yildiz, E. Deniz and F. M. Raymo, *Chem. Soc. Rev.*, 2009, **38**, 1859–1867.
6 D. Kim and S. Y. Park, *Adv. Opt. Mater.*, 2018, **6**, 1800678.
7 H. Ren, D. Chen, Y. Shi, H. Yu and Z. Fu, *Polymer*, 2016, **97**, 533–542.
8 Y. Chen, X. Feng, Z. Sun, D. Wang, T. Yang, Z. Zhao, L. Li, X. Wang and H. Yu, *Chem. – Asian J.*, 2018, **13**, 2781–2785.
9 H. Ren, D. Chen, Y. Shi, H. Yu, Z. Fu and W. Yang, *Macromolecules*, 2018, **51**, 3290–3298.
10 B.-K. An, S.-K. Kwon, S.-D. Jung and S. Y. Park, *J. Am. Chem. Soc.*, 2002, **124**, 14410–14415.
11 B.-K. An, J. Gierschner and S. Y. Park, *Acc. Chem. Res.*, 2012, **45**, 544–554.
12 L. Zhu and Y. Zhao, *J. Mater. Chem. C*, 2013, **1**, 1059–1065.
13 M. Martinez-Abadia, R. Gimenez and M. B. Ros, *Adv. Mater.*, 2018, **30**, 1704161.

14 Y. Hong, J. W. Y. Lam and B. Z. Tang, *Chem. Commun.*, 2009, 4332–4353.
15 Y. Hong, J. W. Y. Lam and B. Z. Tang, *Chem. Soc. Rev.*, 2011, **40**, 5361–5388.
16 J. Mei, N. L. C. Leung, R. T. K. Kwok, J. W. Y. Lam and B. Z. Tang, *Chem. Rev.*, 2015, **115**, 11718–11940.
17 S.-J. Yoon, J. H. Kim, K. S. Kim, J. W. Chung, B. Heinrich, F. Mathevet, P. Kim, B. Donnio, A.-J. Attias, D. Kim and S. Y. Park, *Adv. Funct. Mater.*, 2012, **22**, 61–69.
18 H. Kim and J. Y. Chang, *Langmuir*, 2014, **30**, 13673–13679.
19 M. Martinez-Abadia, S. Varghese, B. Milian-Medina, J. Gierschner, R. Gimenez and M. B. Ros, *Phys. Chem. Chem. Phys.*, 2015, **17**, 11715–11724.
20 S. K. Park, I. Cho, J. Gierschner, J. H. Kim, J. H. Kim, J. E. Kwon, O. K. Kwon, D. R. Whang, J.-H. Park, B.-K. An and S. Y. Park, *Angew. Chem., Int. Ed.*, 2016, **55**, 203–207.
21 V. Palakollu and S. Kanvah, *New J. Chem.*, 2014, **38**, 5736–5746.
22 S.-J. Yoon, J. W. Chung, J. Gierschner, K. S. Kim, M.-G. Choi, D. Kim and S. Y. Park, *J. Am. Chem. Soc.*, 2010, **132**, 13675–13683.
23 C. Dou, L. Han, S. Zhao, H. Zhang and Y. Wang, *J. Phys. Chem. Lett.*, 2011, **2**, 666–670.
24 Y. Zhang, J. Sun, G. Bian, Y. Chen, M. Ouyang, B. Hu and C. Zhang, *Photochem. Photobiol. Sci.*, 2012, **11**, 1414–1421.
25 S.-J. Yoon and S. Park, *J. Mater. Chem.*, 2011, **21**, 8338–8346.
26 Y. Zhang, J. Sun, X. Lv, M. Ouyang, F. Cao, G. Pan, L. Pan, G. Fan, W. Yu, C. He, S. Zheng, F. Zhang, W. Wang and C. Zhang, *CrystEngComm*, 2013, **15**, 8998–9002.
27 Y. Zhang, G. Zhuang, M. Ouyang, B. Hu, Q. Song, J. Sun, C. Zhang, C. Gu, Y. Xu and Y. Ma, *Dyes Pigm.*, 2013, **98**, 486–492.
28 H. Zhao, Y. Wang, S. Harrington, L. Ma, S. Hu, X. Wu, H. Tang, M. Xue and Y. Wang, *RSC Adv.*, 2016, **6**, 66477–66483.
29 Y. Zhang, H. Li, G. Zhang, X. Xu, L. Kong, X. Tao, Y. Tian and J. Yang, *J. Mater. Chem. C*, 2016, **4**, 2971–2978.
30 V. Palakollu and S. Kanvah, *New J. Chem.*, 2014, **38**, 5736–5746.
31 A. Gulino, F. Lupo, G. G. Condorelli, M. E. Fragala, M. E. Amato and G. Scarlata, *J. Mater. Chem.*, 2008, **18**, 5011–5018.
32 L. Zhu, C. Y. Ang, X. Li, K. T. Nguyen, S. Y. Tan, H. Agren and Y. Zhao, *Adv. Mater.*, 2012, **24**, 4020–4024.
33 J. W. Chung, S.-J. Yoon, B.-K. An and S. Y. Park, *J. Phys. Chem. C*, 2013, **117**, 11285–11291.
34 L. Zhu, X. Li, Q. Zhang, X. Ma, M. Li, H. Zhang, Z. Luo, H. Agren and Y. Zhao, *J. Am. Chem. Soc.*, 2013, **135**, 5175–5182.
35 J. Seo, J. W. Chung, J. E. Kwon and S. Y. Park, *Chem. Sci.*, 2014, **5**, 4845–4850.
36 H. Lu, L. Qiu, G. Zhang, A. Ding, W. Xu, G. Zhang, X. Wang, L. Kong, Y. Tian and J. Yang, *J. Mater. Chem. C*, 2014, **2**, 1386–1389.
37 J. W. Park, S. Nagano, S.-J. Yoon, T. Dohi, J. Seo, T. Seki and S. Y. Park, *Adv. Mater.*, 2014, **26**, 1354–1359.
38 P. Xing, H. Chen, L. Bai and Y. Zhao, *Chem. Commun.*, 2015, **51**, 9309–9312.
39 Y. Jin, Y. Xia, S. Wang, L. Yan, Y. Zhou, J. Fan and B. Song, *Soft Matter*, 2015, **11**, 798–805.
40 R. Gao, D. Cao, Y. Guan and D. Yan, *ACS Appl. Mater. Interfaces*, 2015, **7**, 9904–9910.
41 X. Guo, J. Zhou, M. A. Siegler, A. E. Bragg and H. E. Katz, *Angew. Chem., Int. Ed.*, 2015, **54**, 4782–4786.
42 H. Lu, S. Wu, C. Zhang, L. Qiu, X. Wang, G. Zhang, J. Hu and J. Yang, *Dyes Pigm.*, 2016, **128**, 289–295.
43 M. Yang, P. Xing, M. Ma, Y. Zhang, Y. Wang and A. Hao, *Soft Matter*, 2016, **12**, 6038–6042.
44 M. Martinez-Abadia, B. Robles-Hernandez, M. R. de la Fuente, R. Gimenez and M. B. Ros, *Adv. Mater.*, 2016, **28**, 6586–6591.
45 J. W. Chung, Y. You, H. S. Huh, B.-K. An, S.-J. Yoon, S. H. Kim, S. W. Lee and S. Y. Park, *J. Am. Chem. Soc.*, 2009, **131**, 8163–8172.
46 M. Martinez-Abadia, S. Varghese, R. Gimenez and M. B. Ros, *J. Mater. Chem. C*, 2016, **4**, 2886–2893.
47 M. Martinez-Abadia, S. Varghese, P. Romero, J. Gierschner, R. Gimenez and M. B. Ros, *Adv. Opt. Mater.*, 2017, **5**, 1600860.
48 Y. Zhu, M. Zheng, Y. Tu and X.-F. Chen, *Macromolecules*, 2018, **51**, 3487–3496.
49 J. Liao, M. Yang, Z. Liu and H. Zhang, *J. Mater. Chem. A*, 2019, **7**, 2002–2008.
50 Y. Yuan, J. Li, L. He and H. Zhang, *Eur. Polym. J.*, 2018, **105**, 7–16.
51 Y. Yuan, J. Li, L. He, Y. Liu and H. Zhang, *J. Mater. Chem. C*, 2018, **6**, 7119–7127.
52 Q. Li, Y. Yuan, L. He, S. Liu and H. Zhang, *Polym. Chem.*, 2018, **9**, 5521–5530.
53 M. Yang, Z. Liu, B. Yang and H. Zhang, *New J. Chem.*, 2019, **43**, 4205–4215.
54 Y. Yuan, L. He, J. Li and H. Zhang, *Polym. Chem.*, 2019, **10**, 2706–2715.
55 S. Ma, Y. Cai, Y. Tu, Y. Guan and X. Chen, *Polym. Chem.*, 2016, **7**, 3520–3529.
56 S. Xue, X. Qiu, Q. Sun and W. Yang, *J. Mater. Chem. C*, 2016, **4**, 1568–1578.
57 H. Yu, *J. Mater. Chem. C*, 2014, **2**, 3047–3054.
58 J. Hu, X. Li, Y. Ni, S. Ma and H. Yu, *J. Mater. Chem. C*, 2018, **6**, 10815–10821.